NANO LETTERS

Letter

pubs.acs.org/NanoLett

Fano-Like Resonances Arising from Long-Lived Molecule-Plasmon Interactions in Colloidal Nanoantennas

Renee R. Frontiera,* Natalie L. Gruenke, and Richard P. Van Duyne*

Department of Chemistry, Northwestern University, Evanston, Illinois 60208, United States

Supporting Information

ABSTRACT: We examine ultrafast dynamics in a coupled molecule-plasmon system. Using a new ultrafast Raman technique called surface enhanced-femtosecond stimulated Raman spectroscopy (SE-FSRS), we prove that plasmonic nanoparticles and adsorbed molecules are coupled by the appearance of Fano-like lineshapes, which arise from the interaction of narrowband vibrational coherences and the broadband plasmon resonance. We probe the effect of plasmon energy on the vibrational lineshapes and observe changes in the phase of the line shape dispersion. Finally, we examine the effect of plasmon-molecule coupling on the molecular vibrational coherence lifetime. Surprisingly, coupling of the molecular vibration to the plasmon does not significantly shorten the vibrational coherence dephasing time. Better understanding of the ultrafast dynamics of excited vibrational states and vibrational coherences in coupled molecular-plasmonic systems should assist in developing a mechanism-based view of plasmonically enhanced photovoltaic and photocatalytic systems.

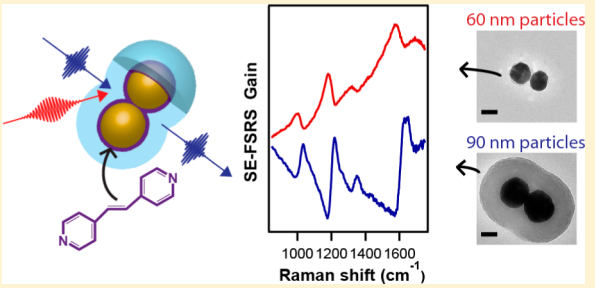

KEYWORDS: *Plasmonics, surface-enhanced Raman scattering, femtosecond stimulated Raman spectroscopy, vibrational coherence lifetimes, molecule-plasmon interactions*

The effect of plasmons on molecular reaction dynamics has far-reaching implications for plasmonically enhanced photocatalysis and photovoltaic devices. A significant number of reports have demonstrated efficiency improvements by the incorporation of plasmonic materials.[1−7] However, the mechanism for these improvements is not entirely clear. It is not yet determined if plasmons affect the rate or yield of chemical reactions or if the benefits simply result from increased scattering and/or temperature. It is possible that nearby plasmonic materials may affect the reaction mechanisms or lifetimes of photoinduced populations, which could be optimized for maximum device performance.

It has long been known that metal surfaces quench nearby molecular excited states due to rapid nonradiative energy transfer to the metal.[8−10] For example, the fluorescence quantum yield from rhodamine 6G drops at least 3 orders of magnitude when adsorbed onto a plasmonic metal surface.[11] This effect enables surface-enhanced resonance Raman spectroscopy (SERRS) of highly fluorescent dye molecules, in which the excited state is typically quenched before fluorescence occurs.[12] A significant body of work has also examined vibrational dynamics at metal surfaces,[13] but less work has addressed the behavior of molecular vibrations near plasmons.

Additionally, given that photocatalytic and photovoltaic devices involve dynamics on an ultrafast time scale, the role of vibrational coherences and other femtosecond and picosecond scale phenomena are likely significant. Coherences are known to play a significant role in energy and electron transfer in biological systems.[14,15] However, the lifetimes of vibrational coherences when in the vicinity of a nearby coupled plasmon have not previously been investigated. It is not known what effects, if any, rapid molecule-plasmon energy transfer has on dephasing times of vibrational coherences in coupled systems.

Here we probe spectrally narrow molecular vibrational coherences and a broadband plasmon mode which are coupled, as demonstrated by the presence of a Fano-like resonance feature. Fano resonances are now frequently observed in plasmonics when examining systems with at least one narrow-bandwidth resonance.[16−19] A Fano resonance arises from interactions between a discrete narrowband state and a broad continuum, resulting in a characteristic asymmetric line shape.[18,20] Frequently this involves interactions between a bright and dark plasmon mode. In order to obtain a narrow plasmon mode, the systems are typically fabricated with lithographic techniques and examined on a single cluster level. To our knowledge, there are no demonstrations of a Fano resonance of plasmonic nanoparticles in a solution, most likely due to the typical heterogeneity of these samples.

Reports investigating Fano resonance-like coupling between molecules and plasmons are much less frequent than those examining coupling between plasmons. Those that exist are mainly presented as a molecular perturbation to the plasmon resonance. There have been several reports of asymmetric

Received: September 19, 2012
Revised: October 15, 2012

   dx.doi.org/10.1021/nl303488m | *Nano Lett.* XXXX, XXX, XXX−XXX

lineshapes arising in surface enhanced infrared absorption (SEIRA),[21−24] but further investigations have perhaps been limited by the challenge of creating mid-IR plasmons. Several reports examined coupling between J-aggregate absorptions and plasmons.[25,26] As plasmonically enhanced photovoltaic and photocatalytic devices show more promise, it is important to consider how plasmonically enhanced electromagnetic fields will affect molecular dynamics on the ultrafast time scale.

In this work we prove that (1) plasmons and molecules are coupled, as demonstrated by the presence of Fano-like lineshapes and (2) this coupling process does not affect the dephasing time of the vibrational coherence. To our knowledge, this is the first demonstration of molecule-plasmon coupling in colloidal solution, as well as the first investigation of the lifetimes of molecular vibrational coherences coupled to a nearby plasmonic nanoparticle.

To examine molecule-plasmon effects on the femtosecond time scale, we recently developed an ultrafast SERS technique, called surface enhanced-femtosecond stimulated Raman spectroscopy (SE-FSRS).[27] This technique is based on femtosecond stimulated Raman spectroscopy (FSRS), which provides structural information of molecules undergoing photochemical reactions on the femtosecond time scale.[28,29] FSRS routinely achieves simultaneous 50 fs temporal resolution and 10 cm^{-1} spectral resolution, with information obtained about structural changes during the dephasing time of molecular vibrational coherences, which typically last at least several hundred femtoseconds in solution. In FSRS, signal is generated through the creation of vibrational coherences. Two laser beams, a picosecond pump pulse and a femtosecond probe pulse, are used for generating the ground state Raman signal. A vibrational coherence is generated by one upward interaction from the pump and one downward interaction from the probe. This coherence undergoes vibrational dephasing due to interactions with the bath as well as ensemble heterogeneity. At some later and unspecified time, there is another field interaction with the pump pulse, thus generating the Stokes-shifted photon. The theory of the FSRS process has been discussed previously,[30] and the effect of Raman pump−probe time-delay in the electronic ground state has been investigated.[31]

Ground state SE-FSRS data were taken with an ultrafast laser system which has been previously described.[27] Briefly, the 800 mW, 800 nm output of a 100 kHz regenerative amplifier (Coherent RegA) is split into the two pulses necessary for femtosecond stimulated Raman experiments. Fifty percent of the amplifier energy is directed through two identical narrow bandpass filters (CVI laser) to generate the picosecond Raman pump pulse at 795 nm. A portion of the remaining amplifier output is used for continuum generation in sapphire, followed by prism compression. This broadband pulse is filtered for the near-infrared region and is used as the probe pulse. The pulses are focused with a 10 cm lens and overlapped spatially and temporally in the sample. Colloidal solutions were contained in either a 1 mm flow cell or 2 mm cell equipped with micro stir bar capabilities in order to rapidly replenish sample in the laser focal volume. The pump pulse is optically chopped so that sequential images of pump-on and pump-off spectra are obtained.[29,32] The coherent signal, intrinsically heterodyned with the probe pulse, is detected with a spectrograph and CCD array (Princeton Instruments SP2538 and PIXIS:100F). Typical powers used in our experiments were 1 nJ/pulse for the Raman pump pulse and 100 pJ/pulse for the probe pulse, and acquisition times were under 5 min for each SE-FSRS spectrum presented here.

Figure 1A shows a schematic depiction of the nanoantennas used in our study. The nanoantennas consist of gold cores and

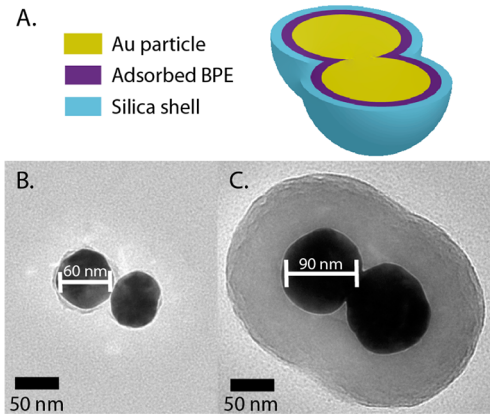

Figure 1. Schematic depiction of nanoantennas (A), consisting of a gold core surrounded by Raman reporter molecules, encapsulated in a silica shell. BPE is *trans*-1,2-bis(4-pyridyl)-ethylene. TEM images of nanoantennas containing 60 nm cores (B) and 90 nm cores (C).

a near-monolayer of adsorbed *trans*-1,2-bis(4-pyridyl)-ethylene (BPE) molecules, all encapsulated in a silica shell. Crucially, the particles are aggregated before silica coating, creating small junctions at the interface of the spheres. These hotspots are responsible for all Raman signals observed in this paper. The size of the cores can be varied, as shown in the TEM images in Figure 1B,C. We refer to the two samples as containing 60-nm- and 90-nm-cores, although there is significant variation in individual particle size. The 90-nm-core sample has been previously characterized to consist of 52% monomers, 10% dimers, 21% trimers, and 17% larger clusters.[33] This work demonstrated that the SERS enhancement factor was independent of aggregation state, and that any clusters containing sub-nanometer gaps or crevices provided the highest magnitude signals. The 60-nm-core sample contains a much larger fraction of monomers, although we do not quantitate it here. The thickness of the silica shell varies dramatically between and within the two samples, but appears to have no effect on the ensemble-averaged SE-FSRS signal.

Changing the diameter of the gold core sizes results in a dramatic change in the bulk plasmon resonance spectrum, as is depicted in Figure 2. Here we show only the region between 700 and 1200 nm, corresponding to the plasmon resonances of the multicore structures. Due to the low concentration of aggregates in the 60-nm-core sample, a broad sloping background from the single-core resonance was subtracted. It is clear that the multicore plasmon mode shifts ∼100 nm between the 60- and 90-nm-core samples. Additionally, the spectra of the pulses used for the experiment are displayed, with the Raman pump spectrum in green and the probe spectrum in purple. Crucially, the probe overlaps with the peak of the 60-nm-nanoantenna plasmon resonance and is on the blue edge of the plasmon resonance for the 90-nm-core sample.

The surface enhanced-femtosecond stimulated Raman spectra for the two nanoantenna samples are displayed in Figure 3. The spectrum from the 90-nm-core sample agrees with our previously published work,[27] consisting of dispersive lineshapes at the BPE vibrational frequencies. Remarkably, the

dx.doi.org/10.1021/nl303488m | *Nano Lett.* XXXX, XXX, XXX−XXX

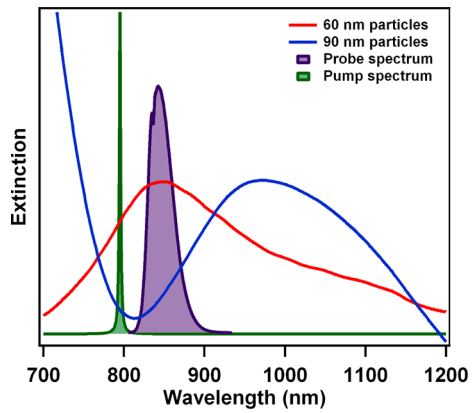

Figure 2. Extinction spectra of the 60- and 90-nm-core nanoantennas used for SE-FSRS experiments. Overlaid are the spectra of the laser pulses used in the experiment; the picosecond duration Raman pump pulse at 795 nm and the femtosecond probe pulse in the near-infrared region.

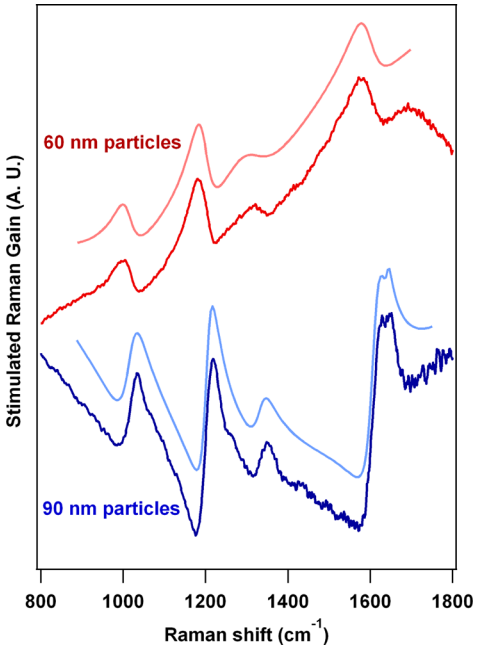

Figure 3. Surface enhanced-femtosecond stimulated Raman spectra of 60- (red) and 90- (blue) nm-nanoantenna colloidal samples. The dispersive Raman features from *trans*-1,2-bis(4-pyridyl)-ethylene change phase depending on the size of the gold spheres. Fits to the data are shown vertically displaced above the spectra. The SE-FSRS data were fit to Fano functions as described in the text and show remarkable agreement with all features seen in the data. The spectra have been scaled for easy comparison.

SE-FSRS signal from the 60-nm-core sample shows similar peaks positions but with oppositely phased dispersion. In the 90-nm-core sample the vibrational features are characterized by a dip on the low cm^{-1} side and a peak on the high cm^{-1} side, while in the 60-nm-core sample the peak is on the low cm^{-1} side. Both spectra additionally have a broad background, which arises from the transient absorption-like response of the plasmon resonance to the Raman pump excitation.[34]

Qualitatively, the dispersive nature of these vibrational features resemble the Fano lineshapes commonly seen between coupled bright and dark plasmons. The changing phase of the dispersion when the plasmon resonance is shifted is also indicative of a Fano resonance. However, in this case, we are observing interactions between a narrow molecular vibrational coherence and a broad plasmon resonance. To support this concept, we fit our spectra to Fano line shape functions,[20] with a broad polynomial background to account for the transient plasmon response. The fitting function for an individual vibrational resonance is in eq 1

$$f(x) = A\left(\frac{\left(q + \frac{x - x_0}{\Gamma/2}\right)^2}{1 + \left(\frac{x - x_0}{\Gamma/2}\right)^2}\right) \quad (1)$$

Here A represents the amplitude of each peak, q is the Fano asymmetry parameter describing the degree of coupling between the single vibrational mode and the plasmon continuum, x_0 is the central frequency of the vibrational feature, and Γ is the line width. The fits are displayed above the data in Figure 3. The peak frequency and width values are reported in Table 1. Despite the complexity and number of terms in the fitting function, we are able to obtain an excellent fit reproducing all the features of the experimental data and Fano-like interaction easily explains the phase shifts in the experimental spectra. In contrast, fitting to a dispersive Lorentzian line shape resulted in weaker agreement with the data.

Table 1. Results from the Fano Fitting of the SE-FSRS Data from BPE Molecules Adsorbed on 90- and 60-nm Gold Core Assemblies[a]

	x_0 (90 nm)	x_0 (60 nm)	Γ (90 nm)	Γ (60 nm)	mode character
peak 1	1018	1011	60	56	ring breathing
peak 2	1204	1196	40	56	ethylenic C=C stretch
peak 3	1334	1310	53	146	CH wag
peak 4*	1610*	1593*	51*	78*	pyridine C=C stretch
peak 5*	1641*	*	15*	*	ethylenic stretch

[a]All values are in cm^{-1}; x_0 is the center frequency and Γ is the linewidth from the fit, according to eq 1. The asterisk indicates two peaks that are very similar in frequency and appeared to be only one peak in the 60 nm data. Values from the starred fits should not be directly compared as the resolution is not sufficient to fit these peaks separately in the 60-nm-core sample. Mode character assignments are from ref 35.

Though it is not possible to decouple the Fano q parameter from the line width and thus vibrational dephasing time in the fit function,[20] we were able to obtain excellent agreement using one value for q for all of the vibrational features in a given sample. For the 90-nm-core sample, SE-FSRS data were best fit with $q = 1.5$, and for the 60-nm-core sample, $q = -1.9$. The reversal of the sign indicates a change in the phase of the dispersion. The increase in the absolute value of q for the 60-nm-core sample is reflected in the broader features in the SE-FSRS spectrum. This is particularly noticeable in the region around 1600 cm^{-1}, where the two peaks visible in the 90-nm-core sample are no longer resolved and instead appear as one broad peak.

Since we set the Fano coupling parameter q to be the same for all vibrations, changes in line width parameter between the samples and for different vibrational features are indicative of changes in either the coupling magnitude or the vibrational

dx.doi.org/10.1021/nl303488m | Nano Lett. XXXX, XXX, XXX−XXX

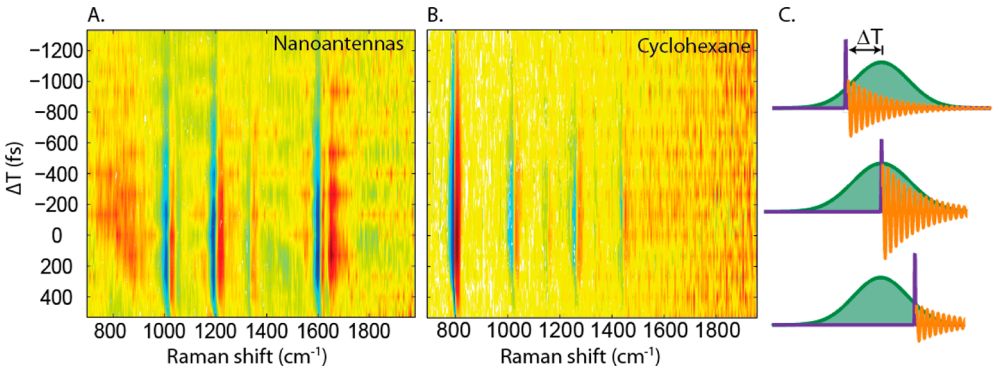

Figure 4. SE-FSRS data examining time-delay dependence between the pump and probe pulses, for both the 90-nm-nanoantenna sample (A) and the neat cyclohexane standard (B). A schematic depiction of the time-delay experiment is shown in panel C, where changing the time delay between the pump (green) and probe (purple) pulse temporal maxima changes the truncation of the detected vibrational coherence (orange). The Raman spectra for both the nanoantennas and the cyclohexane standard show characteristic peaks which persist for the same duration of time. The identical behavior of the Raman features as a function of Raman pump−probe time delay indicates that the dephasing is limited only by the picosecond time scale of the experiment. The spectra are presented as a derivative of the data in order to minimize features from the broadly sloping transient absorption background. Thus red features represent a positive slope in the original data, and blue represents a negative slope. The color scale is in arbitrary units and has been adjusted for maximum comparison between the two samples.

coherence lifetime. There are at least two possible mechanisms which could give rise to these changes. First, there could be a mode symmetry effect on the coupling or dephasing time of the coherence near a plasmon. Of the first three well-separated peaks, the two in-plane vibrational modes, around 1010 and 1200 cm^{-1}, have nearly the same width. The one out-of-plane mode, around 1330 cm^{-1}, peak 3, shows a significant increase in line shape width for the 60 nm core sample as compared to the 90 nm sample. However, the few peaks observed here make it challenging to draw any definite conclusions relating the mode character to the degree of coupling and/or dephasing.

A more likely explanation for the line width variance is that it results from changes in the energy of the vibrational feature relative to the peak of the plasmon resonance. For the 90 nm sample, the plasmon resonance maximum is well to the red of the probe pulse and all of the vibrational modes. Since the slope of the plasmon resonance is relatively constant throughout the Stokes region, it is unsurprising that all of the Fano-like features have similar widths and line shapes. However, for the 60 nm sample, the probe spectrum and vibrational peaks straddle the peak of the plasmon resonance. The 1010 cm^{-1} Raman shift occurs at ∼860 nm, near the peak on the plasmon resonance, whereas the 1310 cm^{-1} Raman peak occurs at ∼880 nm, on the downward slope of the plasmon resonance. This change in the slope of the plasmon resonance across the vibrational spectrum likely results in subtle changes in the line shape, as has been observed previously.[21] Future work including a wider range of plasmon resonance energies will examine this connection more closely.

In order to investigate the nature of this Fano-like interaction, we probed the ultrafast response of the nanoantennas. To examine the dephasing time of a vibrational coherence coupled to a plasmon more thoroughly, we explored the effect of pump−probe time delay on the SE-FSRS spectra. Previous experimental and theoretical work thoroughly examined line shape changes in nonsurface enhanced-FSRS as a function of Raman pump−probe time-delay.[31,36,37] The observed results can be explained by consideration of the truncation time of the vibrational dephasing time. When the femtosecond probe pulse occurs after the picosecond pump pulse temporal maximum, the detected vibrational coherence is truncated early, and the vibrational peaks appear wider. When the probe pulse occurs early in the pump pulse duration, the peaks are narrower due to full sampling of the vibrational coherence time. The peak intensity maximum occurs approximately when the pulses are overlapped at their temporal maxima, at the point of the most efficient generation of coherence. By convention, we define a negative time delay as one in which the probe precedes the temporal maximum of the pump pulse.[31]

The time-delay spectra for the 90-nm-core sample are presented in Figure 4a, with similar data from neat cyclohexane presented in Figure 4b to indicate the instrument response. There is a broad transient absorption-like baseline from the nanoantenna plasmon resonance. Thus we present the derivative of the data in order to emphasize vibrational features above the slowly varying background signal. The original data are presented in the SI. Vibrational features are characterized by the blue (negative slope in original data) and red (positive slope) vertical stripes in the spectra, and are most intense when the pump and probe temporal maxima are overlapped, at $\Delta T = 0$. The vibrational signals at positive time delays are broadened slightly due to truncation of the detected vibrational coherence. Signal from the nanoantennas persists for a similar amount of time as compared to the neat cyclohexane standard, indicating that the behavior is temporally long and limited by the instrument response. Surprisingly, there is no change in line shape across all temporal regions probed; the vibrational features from the nanoantennas remain dispersive for all time delays.

We observe no significant changes in the nanoantenna line shapes with changes in the pump−probe time delay. This lack of line shape change indicates that the signals result from coupling and not simply the sum of multiple interfering signals in the third-order polarization. We can rule out interference resulting merely from a third-order polarization response consisting of separate molecular and plasmonic terms as the origin of our dispersive line shape because we would expect to see changes in the dispersion as the time delay is changed, similar to those observed in FSRS and CARS.[37−39] Since the vibrational line shapes do not change with time delay, we believe the dispersive nature of our signals result from Fano-like

dx.doi.org/10.1021/nl303488m | Nano Lett. XXXX, XXX, XXX−XXX

couplings between the molecule and plasmon, and do not result from interference from any plasmon-only four-wave mixing signals which combine with the vibrational signal on the detector.

Surprisingly, the coupling to the nearby plasmon has no observable effect on the vibrational dephasing time, since the lifetimes in the time-dependent spectra are similar for both cyclohexane and BPE nanoantennas. The pump−probe time-delay range over which we see signal for the 90 nm nanoantennas has a FWHM of 900 fs, as determined by a fit to the 1200 cm^{-1} peak amplitude (see SI). This behavior indicates that there is no quenching of the vibrational coherence by the metal plasmon, at least as can be observed by our instrument. Additionally, the relatively narrow vibrational features observed in SE-FSRS indicate a coherence lifetime of several hundred femtoseconds. This is unexpected, since the nearby coupled plasmon is a significant energy sink for the vibrational coherence. After creation, no additional energy is added to the coherence, yet even though it could readily transfer energy to the nearby coupled plasmon, the lifetime is not shortened. It is possible that the simultaneous excitation of the plasmon promotes the existence of the coherence significantly beyond the probe pulse duration. Future theoretical work is needed to examine the details of this coupling mechanism, as well as to consider why SE-FSRS shows Fano line shapes while SERS does not.

In summary, we have shown that the coupling between colloidal nanoparticles and adsorbed molecules results in a Fano-like line shape in SE-FSRS. The vibrational features from BPE in SE-FSRS are dispersive, and the phase of the dispersion switches as the plasmon energy is varied. We fit these line shapes to a Fano function and are able to extract line width and coupling information. Surprisingly, we observe that the coupling to the plasmon has little to no effect on the vibrational coherence lifetime of the molecule. This work indicates that plasmonically enhanced photochemistry can involve reactions with long-lived vibrational coherences or vibrationally excited states, and is a first step toward a mechanistic understanding of plasmonically enhanced photocatalysis and photodriven electron transfer.

■ ASSOCIATED CONTENT

Supporting Information

Additional TEM images, SE-FSRS time-delay data and data processing information, and fits to time-delay data. This material is available free of charge via the Internet at http://pubs.acs.org.

■ AUTHOR INFORMATION

Corresponding Author

*E-mail: rfrontiera@northwestern.edu; vanduyne@northwestern.edu.

Author Contributions

The manuscript was written through contributions of all authors. All authors have given approval to the final version of the manuscript.

Notes

The authors declare no competing financial interest.

■ ACKNOWLEDGMENTS

We thank Dr. R. Griff Freeman and Dr. Michael J. Natan from Cabot Security Materials, Inc. for providing the nanoantennas. This work was supported by the National Science Foundation (CHE-0802913, CHE-0911145, CHE-1152547, and DMR-1121262), AFOSR/DARPA Project BAA07-61 (FA9550-08-1-0221), and the Department of Energy Basic Energy Sciences (DE-FG02-09ER16109 and DE-FG02-03ER15457). TEM experiments were performed in the EPIC Facility of the NUANCE Center at Northwestern University. NUANCE is supported by the NSF-NSEC, NSF-MRSEC, Keck Foundation, State of Illinois, and Northwestern University. N.L.G. acknowledges support from the National Science Foundation Graduate Research Fellowship Program under Grant No. DGE-0824162.

■ ABBREVIATIONS

SE-FSRS, surface enhanced-femtosecond stimulated Raman spectroscopy; SERS, surface enhanced Raman spectroscopy; FSRS, femtosecond stimulated Raman spectroscopy; EM, electromagnetic; TEM, transmission electron microscopy; BPE, *trans*-1,2-bis(4-pyridyl)-ethylene; FWHM, full width at half maximum

■ REFERENCES

(1) Atwater, H. A.; Polman, A. *Nat. Mater.* **2010**, *9* (3), 205−213.
(2) Schuller, J. A.; Barnard, E. S.; Cai, W.; Jun, Y. C.; White, J. S.; Brongersma, M. L. *Nat. Mater.* **2010**, *9* (3), 193−204.
(3) Wang, D. H.; Kim, D. Y.; Choi, K. W.; Seo, J. H.; Im, S. H.; Park, J. H.; Park, O. O.; Heeger, A. J. *Angew. Chem., Int. Ed.* **2011**, *50* (24), 5519−5523.
(4) Pillai, S.; Catchpole, K. R.; Trupke, T.; Green, M. A. *J. Appl. Phys.* **2007**, *101*, (9).
(5) Hung, W. H.; Aykol, M.; Valley, D.; Hou, W.; Cronin, S. B. *Nano Lett.* **2010**, *10* (4), 1314−1318.
(6) Ingram, D. B.; Linic, S. *J. Am. Chem. Soc.* **2011**, *133* (14), 5202−5205.
(7) Zhou, X.; Andoy, N. M.; Liu, G.; Choudhary, E.; Han, K.-S.; Shen, H.; Chen, P. *Nat. Nanotechnol.* **2012**, *7* (4), 237−241.
(8) Waldeck, D. H.; Alivisatos, A. P.; Harris, C. B. *Surf. Sci.* **1985**, *158* (1−3), 103−125.
(9) Gersten, J.; Nitzan, A. *J. Chem. Phys.* **1981**, *75* (3), 1139−1152.
(10) Pockrand, I.; Brillante, A.; Mobius, D. *Chem. Phys. Lett.* **1980**, *69* (3), 499−504.
(11) Ritchie, G.; Burstein, E. *Phys. Rev. B: Condens. Matter* **1981**, *24* (8), 4843−4846.
(12) Stiles, P. L.; Dieringer, J. A.; Shah, N. C.; Van Duyne, R. P. *Annu. Rev. Anal. Chem.* **2008**, *1*, 601−626.
(13) Arnolds, H. *Prog. Surf. Sci.* **2011**, *86* (1−2), 1−40.
(14) Engel, G. S.; Calhoun, T. R.; Read, E. L.; Ahn, T.-K.; Mancal, T.; Cheng, Y.-C.; Blankenship, R. E.; Fleming, G. R. *Nature* **2007**, *446* (7137), 782−786.
(15) Vos, M. H.; Rappaport, F.; Lambry, J. C.; Breton, J.; Martin, J. L. *Nature* **1993**, *363* (6427), 320−325.
(16) Fan, J. A.; Bao, K.; Wu, C.; Bao, J.; Bardhan, R.; Halas, N. J.; Manoharan, V. N.; Shvets, G.; Nordlander, P.; Capasso, F. *Nano Lett.* **2010**, *10* (11), 4680−4685.
(17) Lassiter, J. B.; Sobhani, H.; Fan, J. A.; Kundu, J.; Capasso, F.; Nordlander, P.; Halas, N. J. *Nano Lett.* **2010**, *10* (8), 3184−3189.
(18) Luk'yanchuk, B.; Zheludev, N. I.; Maier, S. A.; Halas, N. J.; Nordlander, P.; Giessen, H.; Chong, C. T. *Nat. Mater.* **2010**, *9* (9), 707−715.
(19) Ye, J.; Wen, F.; Sobhani, H.; Lassiter, J. B.; Van Dorpe, P.; Nordlander, P.; Halas, N. J. *Nano Lett.* **2012**, *12* (3), 1660−1667.
(20) Fano, U. *Phys. Rev.* **1961**, *124* (6), 1866−1878.
(21) Neubrech, F.; Pucci, A.; Cornelius, T. W.; Karim, S.; Garcia-Etxarri, A.; Aizpurua, J. *Phys. Rev. Lett.* **2008**, *101*, (15).
(22) Bjerke, A. E.; Griffiths, P. R.; Theiss, W. *Anal. Chem.* **1999**, *71* (10), 1967−1974.
(23) Priebe, A.; Sinther, M.; Fahsold, G.; Pucci, A. *J. Chem. Phys.* **2003**, *119* (9), 4887−4890.

(24) Adato, R.; Yanik, A. A.; Amsden, J. J.; Kaplan, D. L.; Omenetto, F. G.; Hong, M. K.; Erramilli, S.; Altug, H. *Proc. Natl. Acad. U.S.A.* **2009**, *106* (46), 19227−19232.
(25) Wiederrecht, G. P.; Wurtz, G. A.; Bouhelier, A. *Chem. Phys. Lett.* **2008**, *461* (4−6), 171−179.
(26) Kelley, A. M. *Nano Lett.* **2007**, *7* (10), 3235−3240.
(27) Frontiera, R. R.; Henry, A.-I.; Gruenke, N. L.; Van Duyne, R. P. *J. Phys. Chem. Lett.* **2011**, *2* (10), 1199−1203.
(28) Kukura, P.; McCamant, D. W.; Mathies, R. A. *Annu. Rev. Phys. Chem.* **2007**, *58*, 461−488.
(29) Frontiera, R. R.; Fang, C.; Dasgupta, J.; Mathies, R. A. *Phys. Chem. Chem. Phys.* **2012**, *14* (2), 405−414.
(30) Lee, S. Y.; Zhang, D. H.; McCamant, D. W.; Kukura, P.; Mathies, R. A. *J. Chem. Phys.* **2004**, *121* (8), 3632−3642.
(31) Yoon, S.; McCamant, D. W.; Kukura, P.; Mathies, R. A.; Zhang, D. H.; Lee, S. Y. *J. Chem. Phys.* **2005**, *122*, 2.
(32) McCamant, D. W.; Kukura, P.; Yoon, S.; Mathies, R. A. *Rev. Sci. Instrum.* **2004**, *75* (11), 4971−4980.
(33) Wustholz, K. L.; Henry, A.-I.; McMahon, J. M.; Freeman, R. G.; Valley, N.; Piotti, M. E.; Natan, M. J.; Schatz, G. C.; Van Duyne, R. P. *J. Am. Chem. Soc.* **2010**, *132* (31), 10903−10910.
(34) Hartland, G. V. *Annu. Rev. Phys. Chem.* **2006**, *57*, 403−430.
(35) Yang, W. H.; Hulteen, J.; Schatz, G. C.; VanDuyne, R. P. *J. Chem. Phys.* **1996**, *104* (11), 4313−4323.
(36) Niu, K.; Cong, S.; Lee, S.-Y. *J. Chem. Phys.* **2009**, *131*, (5).
(37) Frontiera, R. R.; Shim, S.; Mathies, R. A. *J. Chem. Phys.* **2008**, *129*, (6).
(38) Pestov, D.; Murawski, R. K.; Ariunbold, G. O.; Wang, X.; Zhi, M.; Sokolov, A. V.; Sautenkov, V. A.; Rostovtsev, Y. V.; Dogariu, A.; Huang, Y.; Scully, M. O. *Science* **2007**, *316* (5822), 265−268.
(39) Roy, S.; Meyer, T. R.; Gord, J. R. *Appl. Phys. Lett.* **2005**, *87*, (26).